



# Teleconnection of rainfall time series in the central Nile Basin with sea surface temperature

H. Yasuda<sup>1</sup> · S. N. Panda<sup>1,2</sup> · Mohamed A. M. Abd Elbasit<sup>3</sup> · T. Kawai<sup>4</sup> · T. Elgamri<sup>5</sup> · A. A. Fenta<sup>1</sup> · H. Nawata<sup>6</sup>

Received: 22 November 2016 / Revised: 19 May 2017 / Accepted: 25 July 2018 / Published online: 11 August 2018  
© The International Society of Paddy and Water Environment Engineering and Springer Japan KK, part of Springer Nature 2018

## Abstract

We investigated teleconnections of rainfall time series in the central Nile Basin (Sudan and South Sudan) with localities in the global sea surface temperature (SST) field, using monthly rainfall data from 11 gauging stations from 1960 to 1999. Annual rainfall ranged from 100 mm in the north to more than 700 mm in the south, and all stations had a strong contrast between rainy and dry seasons with rainless dry periods of several months. Rainfall time series at the stations were categorized as strongly seasonal, with precipitation concentration index exceeding 16 and seasonality index exceeding 0.9. The rainfall stations were classified into four zones on the basis of annual rainfall, seasonality, and cross-correlations among the stations. We calculated cross-correlations of interannual rainfall time series in summer (July and August) with the global SST field. For short lag times (0 or 1 month), summer rainfall in Zones I and II (northern arid regions) had significant correlations with SST over the eastern Mediterranean Sea and southern Indian Ocean, summer rainfall in Zone III (semiarid region) had significant negative correlations with SST over the Indian Ocean, and summer rainfall in Zone IV (southern wet region) had significant correlations with SST over tropical areas and the southwestern Pacific Ocean. For long lag times (3–6 months), Nile Basin summer rainfall time series had significant correlations with SST in various regions of the Atlantic and Indian Oceans but not the Pacific Ocean. Rainfall in Zones I and II had positive correlations (significance level < 0.01) with SST south of Greenland and around the Azores Islands and negative correlations with SST south of Madagascar; rainfall in Zone III had negative correlations with SST in parts of the Indian Ocean; and rainfall in Zone IV had significant positive correlations with SST southwest of South Africa and negative correlations with SST in the southwestern Indian Ocean. In sum, rainfall in three of the zones (I, II, and IV) had significant positive and negative correlations with SST in parts of the Indian and Atlantic Oceans. For each of these zones, one positive correlation and one negative correlation were selected and correlations with the time series of the difference between the two SST records were calculated. Correlations of Nile Basin rainfall with the SST differences were stronger than the original positive and negative correlations. The resulting time series of SST difference were applied to an artificial neural network to predict summer rainfall, yielding satisfactory correlation coefficients between the observed and predicted summer rainfall ( $r > 0.70$ ).

**Keywords** ANN · Arid region · Nile Basin · Rainfall time series · SST difference · Teleconnection

✉ H. Yasuda  
hyasd@tottori-u.ac.jp

<sup>1</sup> Division of Environmental Conservation, Arid Land Research Center, Tottori University, 1390 Hamasaka, Tottori 680-0001, Japan

<sup>2</sup> National Institute of Technical Teachers Training and Research, Taramani, Chennai 600 113, India

<sup>3</sup> Institute for Soil, Climate, and Water-Agricultural Research Council, 600 Belvedere Street, Arcadia, Pretoria 0001, South Africa

<sup>4</sup> Arid Land Research Center, Tottori University, Hamasaka 1390, Tottori 680-0001, Japan

<sup>5</sup> Environment Natural Resources and Desertification Research Institute, P.O. 728, Mohamed Nageeb Street, Khartoum, Sudan

<sup>6</sup> Faculty of International Resource Sciences, Akita University, 1-1 Tegata Gakuen-machi, Akita City 010-8502, Japan

## Introduction

The middle reach of the Nile River (Sudan and South Sudan) extends from northern arid regions to southern wet regions. The northern region is a part of the Sahara Desert with annual rainfall of less than 100 mm, whereas annual rainfall in the southern region is nearly 1000 mm. In Sudan, drought is an annual occurrence (Elagib and Elhag 2011). The capital of Sudan, Khartoum, is located at the junction of the Blue Nile and White Nile, whose catchment areas lie in Ethiopia and mainly in Uganda and Kenya, respectively. Rain-fed agriculture is practiced in these areas, and therefore, uncertainty associated with rainfall variability strongly affects their agricultural productivity and natural habitats (Willcocks and Twomlow 1992; Larsson 1996). In Sudan, sharp fluctuations in rainfall hamper its evaluation, and climate change has commonly resulted in delayed onset and reduced duration of the rainy season (Elagib 2011).

Researchers have investigated teleconnections of rainfall time series with sea surface temperature (SST) and atmospheric pressure gradients to evaluate rainfall fluctuations in arid lands. Teleconnections with climate phenomena measured by indices such as the Southern Oscillation Index (SOI), Northern Atlantic Oscillation (NAO), and Indian Ocean Dipole (IOD) have strong influences on regional climate around the world (Uvo et al. 1998; Smith et al. 2000; Behera and Yamagata 2001; Osman and Shamseldin 2002; Saji and Yamagata 2003; Rodríguez-Fonseca et al. 2006; Yasuda et al. 2009; Diro et al. 2011; Chen and Georgakakos 2015; Yuan et al. 2015). Diro et al. (2011) detected teleconnections for summer rainfall in northeastern Ethiopia involving negative correlations with the eastern equatorial Pacific Ocean and with the southwestern Pacific Ocean (northeast of Australia to north of New Zealand).

El Niño and La Niña are occurrences of anomalously warm and cool SST, respectively, in the eastern Pacific Ocean. They correspond to an atmospheric index, the SOI, that expresses an oscillation in sea surface air pressure between the tropical eastern and western Pacific Ocean. The SOI is defined by the air pressure difference between Tahiti and Darwin, Australia. The NAO, defined as the difference in atmospheric pressure at sea level between the Icelandic low and the Azores high, is an indicator of atmospheric circulation over the northern Atlantic Ocean that explains meteorological fluctuations mainly

in Europe and Africa. The IOD is based on the SST difference between the western and eastern Indian Ocean. Its positive phase represents higher-than-average SST and greater precipitation in the western Indian Ocean, with corresponding cooler and drier conditions in the eastern Indian Ocean. The opposite conditions are indicated by the negative phase of the IOD. The Subtropical Indian Ocean Dipole (SIOD) is a similar index emphasizing the southern hemisphere, reflecting the oscillation of SST between the waters south of Madagascar and off western Australia. Its positive phase represents warmer water south of Madagascar and cooler water off western Australia.

It is well established that the world climate is under the strong influence of SST. The influence of SST in the eastern equatorial Pacific Ocean on the climate of Africa was reported by the World Meteorology Organization (2004). Osman and Shamseldin (2002) reported that 34 and 21% of the annual rainfall variability in the central and southern regions of Sudan, respectively, are under the influence of El Niño–Southern Oscillation (ENSO) and the Indian Ocean SST. The interannual time series of June–September rainfall in Ethiopia and Sudan are governed by the Indian summer monsoon (Camberlin 1997). Hameed and Riemer (2012) reported that about 50% of the variance of July–September rainfall in the Sahel (the region from 10°–20°N and 20°W–35°E) is explained by changes in the Azores high and the South Asia low.

Time series of the difference in SSTs between two regions may have highly significant correlations with rainfall time series. Behera and Yamagata (2001) showed that rainfall over many regions in south–central Africa is correlated with cold SST anomalies off Australia and warm SST anomalies south of Madagascar (positive SIOD). Thermal contrasts (SST differences) between the Mediterranean Sea and Indian Ocean are synchronous with rainfall anomalies over the whole Sudan-Sahel belt (Fontaine et al. 2011). Shankar et al. (2007) reported that SST difference between two regions over the Bay of Bengal associates convection and causes rainfall event. Zheng et al. (2014) found that summer monsoon in East Asia is subject to the North Pacific Ocean dipole that is defined as the difference between SST anomaly of the North Pacific (120°–160°E, 36°–44°N) and the Indo-Pacific warm pool (80°–130°E, 4°–24°N). Yasuda et al. (2009) found that the summer rainfall time series from the Chinese Loess Plateau have positive and negative correlations with SST in two Pacific Ocean regions, and the correlation of the

difference between these two SST time series with rainfall is stronger than the correlations of rainfall with the individual regions.

Although the central Nile Basin has possibilities for more productive agriculture, its potential remains latent because of unsuitable water resources. Better knowledge of rainfall fluctuations should contribute to more efficient water management in this region. Summer irrigation is crucial to agriculture here. If a teleconnection between Sudan summer rainfall and SST could be established and rainfall could be predicted, water management in the agricultural sector would be greatly enhanced. However, research on this subject is sparse.

In this study, we investigated the seasonality of rainfall time series in the central Nile Basin and evaluated teleconnections between the rainfall and global SST. We evaluated correlations between rainfall and the SST difference between two sea regions. Finally, we attempted predictions of summer rainfall using an artificial neural network (ANN), a non-linear model that has been applied extensively in hydrology, climatology, and water resources (Uvo et al. 2000; Olsson et al. 2001; Nilsson et al. 2006; Srivastava et al. 2006; Yasuda et al. 2009; Dash et al. 2010; Goyal and Ojha 2012; Singh and Borah 2013).

## Study area and data

This study used monthly rainfall data from 11 gauging stations for 40 years (1960–1999) due to the availability of meteorological data (Fig. 1). The common period when data were fully completed at all stations, 1960–1999, was selected. These stations (with their average annual rainfall) are located at Atbara (59.8 mm), Khartoum (138.1 mm), Kassala (253.9 mm), Medani (311.1 mm), Gadaref (346.0 mm), Sennar (359.6 mm), Kosti (394.2 mm), EL Nahud (430.5 mm), Nyala (565.5 mm), Kadugli (699.0 mm), and Malakal (750.4 mm). There is a wide range in rainfall from 59.8 mm at the northernmost station, Atbara, to 750.4 mm at the southernmost, Malakal. Annual rainfall increases to the south toward the source of the White Nile, and to the east toward the Ethiopian highlands, which is the source of the Blue Nile.

For SSTs, this study used monthly SST data of the Hadley Centre Global Sea Ice and Sea Surface Temperature (HadISST) dataset (Rayner et al. 2003, 2006). The HadISST is provided by the Met Office, UK. The HadISST is monthly

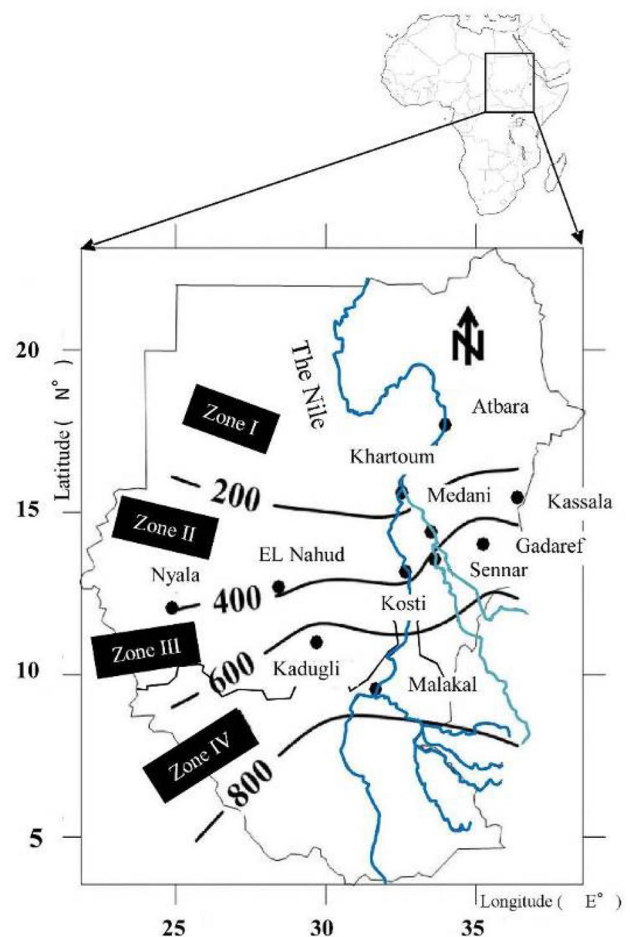


**Fig. 1** Location map showing rainfall stations in the central Nile Basin (dots) and isohyetal lines of mean annual rainfall (in mm)

globally complete fields of SST on a  $1^\circ$  latitude–longitude grid from 1870 to date. Observed data are quality-controlled and interpolated onto a  $1^\circ$  area grid. Individual ships' observations from the Met Office Marine Data Bank (MDB) were quality-controlled and interpolated onto a  $1^\circ$  area grid (Rayner et al. 2003).

## Methodology

### Seasonality of rainfall

As indices to quantify rainfall seasonality, Elagib (2011) applied the precipitation concentration index (PCI) and the

seasonality index (SI) to rainfall time series of arid areas in northern Sudan. In this study, these two indices were used to evaluate seasonality of rainfall at the 11 stations.

The PCI was advocated by Oliver (1980) and has been widely used as an index to evaluate fluctuation of rainfall (Michiels et al. 1992; Apaydin et al. 2006; de Luis et al. 2010, 2011; Kumbuyo et al. 2014). The PCI is calculated as:

$$PCI = 100 \sum_{n=1}^{n=12} \left( \frac{R_n^2}{SR^2} \right) \tag{1}$$

where  $n$  is the observation month (1–12), SR is the annual rainfall, and  $R_n$  is the rainfall of month number  $n$ . The index is classified as uniform (PCI=8.3–10), moderately seasonal (PCI=10–15), seasonal (PCI=15–20), highly seasonal (PCI=20–50), and irregular (PCI=50–100).

The SI was advocated by Ayoade (1970) and has been widely used as an index to evaluate rainfall fluctuation (Bello 1998; Sumner et al. 2001; Livada and Asimakopoulos 2005; Pryor and Schoof 2008). The SI is given as:

$$SI = \frac{1}{SR} \sum_{n=1}^{n=12} \left| R_n - \frac{SR}{12} \right| \tag{2}$$

The index is classified as very equable (SI < 0.19); equable with a definite wetter season (0.20 < SI < 0.39); rather seasonal with a short drier season (0.40 < SI < 0.59); seasonal (0.60 < SI < 0.79); markedly seasonal with a long drier season (0.80 < SI < 0.99); most rain in 3 months or less (1.00 < SI < 1.19); and extremely seasonal (almost all rain in 1–2 months) where SI ≥ 1.20.

Table 1 lists PCI and SI values for the rainfall time series of our 11 stations. For all stations, PCI is greater than 15 and SI is greater than 0.9. In this study, two classifications of PCI and SI are unified. On the SI value, SI < 1.0: ‘seasonal,’ 1.0 < SI < 1.2: ‘highly seasonal,’ and 1.2 < SI: ‘extreme seasonal.’ Division between ‘seasonal’ and ‘highly seasonal’ accords with the PCI value 20 and annual rainfall 600 mm. Another division between ‘extreme seasonal’ and ‘highly seasonal’ accords with the annual rainfall 200 mm. This range classifies the two northern stations (Atbara and Khartoum) as extreme seasonal; the seven central stations (Kassala, Medani, Kosti, El Nahud, Nyala, Sennar, and Gadaref) as highly seasonal; and the two southern stations (Kadugli and Malakal) as seasonal.

### Artificial neural network

We used an artificial neural network (ANN) to predict summer rainfall over Sudan from SST. The ANN has been used for hydrological prediction by plethora of researchers (Uvo et al. 2000; Yasuda et al. 2009; Goyal and Ojha 2012; Singh

Table 1 Precipitation concentration index PCI and seasonality index SI of 11 stations

Station	Zone I		Zone II			Zone III			Zone IV			
	Atbara	Atbara	Khartoum	Kassala	Medani	Kosti	El Nahud	Nyala	Sennar	Gadaref	Kadugli	Malakal
Annual rainfall (mm)	59.8	59.8	138.1	253.9	311.1	346.0	359.6	394.2	430.5	565.5	699.0	750.4
Rainfall range (mm)	0–200	0–200	0.60	200–400	0.27	0.24	0.23	0.28	400–600	0.25	600–	0.16
CV	0.83	0.83	29.45	0.32	25.32	24.70	23.94	23.10	0.25	23.76	0.21	0.16
PCI	32.17	32.17	1.25	24.63	1.12	1.16	1.14	1.13	1.13	1.15	17.73	16.04
SI	1.25	1.25	1.25	1.16	1.12	1.16	1.14	1.13	1.13	1.15	0.95	0.90
		Extreme seasonal		Highly seasonal								Seasonal

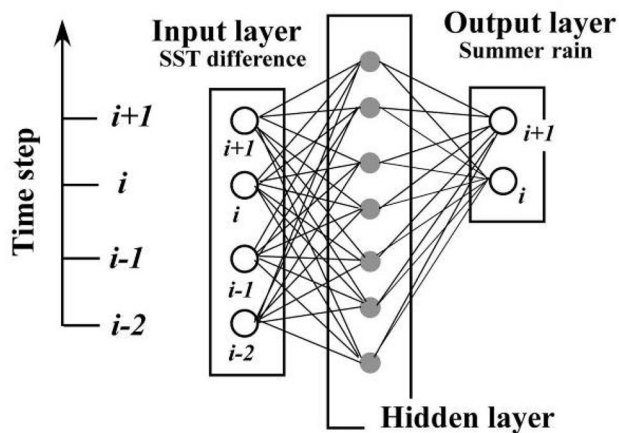


**Fig. 2** Schematic diagram of the structure of the ANN; 4, 7, and 2 neurons at the input, hidden and output layer, respectively. SST difference for 4 years is applied to neurons at the input layer, and the neurons at the hidden layer transfer the input data to the output layer. Two neurons at the output layer are corresponding to summer rainfall for 2 years

and Borah 2013). Since the ANN is a non-dynamic model, it combines two different items like SST and rainfall.

The structure of the ANN consists of input, hidden, and output layers (Fig. 2). There are two neurons in the output layer (corresponding to summer rainfall for 2 years: time step  $i$  and  $i+1$ ) and four neurons in the input layer (corresponding to the SST difference for 4 years; time step:  $i-2$ ,  $i-1$ ,  $i$ , and  $i+1$ ). Seven neurons are used in the hidden layer. Neurons in different layers are connected by weight functions that were optimized by a back-propagation process. The neurons in the hidden layer transfer the input data (SST difference) to the output layer (summer rainfall).

## Data analysis

### Rainfall

Figure 3 presents the mean monthly rainfall and coefficient of variance (CV) of the 11 stations. There is a clear contrast between the rainy and dry seasons. Rainfall occurs only during the rainy season. The total annual rainfall at Kadugli and Malakal is highest among the 11 stations, but the monthly contribution from November to March is very limited. The CV is larger during rainy season months at Atbara and Khartoum, in the north, and during dry season months at Kadugli

and Malakal, in the south. At the other nine stations, rainfall is concentrated in July and August.

The two northernmost stations (Atbara and Khartoum) and southernmost stations (Kadugli and Malakal) in the study area have monthly rainfall distributions that differ from those of the other seven stations. The rainy season is July–August at Atbara and July–September at Khartoum. At Kadugli and Malakal, monthly rainfall is more than 10 mm from April to October. In the central region (Kassala, Medani, Kosti, El Nahud, Nyala, Sennar, and Gadaref), rainfall only occurs from May to October.

Figure 4 presents the annual rainfall, mean annual rainfall, and CV at all 11 stations. All stations display large fluctuations. The early 1980s were dry at all stations, and the drought was especially serious in 1984. Barring and Hulme (1991) reported that the climate of Sudan was dry in 1984 and wet in 1988, even in the northern arid area, including Atbara and Khartoum, where drought conditions prevailed from 1980 to early 1990. The maximum rainfall occurred in 1988. Figure 4 (below right side) shows an inversely proportional relationship between mean annual rainfall and CV (Yasuda et al. 2009; Nicholson 2011). In the northern stations Atbara and Khartoum, the CV is greater than 0.6 and greater than at other stations.

### Divisions of the study area

Zonal division on the basis of mean annual rainfall is a common way in the field of meteorology and hydrology (Rishmawi et al. 2016; Middleton and Thomas 1997; Traore et al. 2012). The mean annual rainfall has a deterministic role on vegetation distribution, farming plan, and evaluation of desertification. Traore et al. (2012) studied Acacia woodlands in the Sudano-Sahelian zone and divided the climatic conditions with mean annual precipitation. Rishmawi et al. (2016) reported a relationship between vegetation and annual rainfall in sub-Saharan and found an evident significant relationship around the 700 mm annual rainfall isohyet.

Researchers have taken various approaches to analyzing Sudan by subregion. Osman and Shamseldin (2002) divided Sudan into four geographic zones strictly by latitude: the desert zone north of latitude  $17^{\circ}\text{N}$ , the semi-desert zone between  $15^{\circ}\text{N}$  and  $17^{\circ}\text{N}$ , the savannah zone between  $9^{\circ}\text{N}$  and  $15^{\circ}\text{N}$ , and the equatorial zone south of  $9^{\circ}\text{N}$ . Elagib and Mansell (2000) and Elagib and Elhag (2011) used rainfall seasonality to divide Sudan into a southern region (south of  $10^{\circ}\text{N}$ ), central region ( $10^{\circ}$ – $16^{\circ}\text{N}$ ), northern region (north of



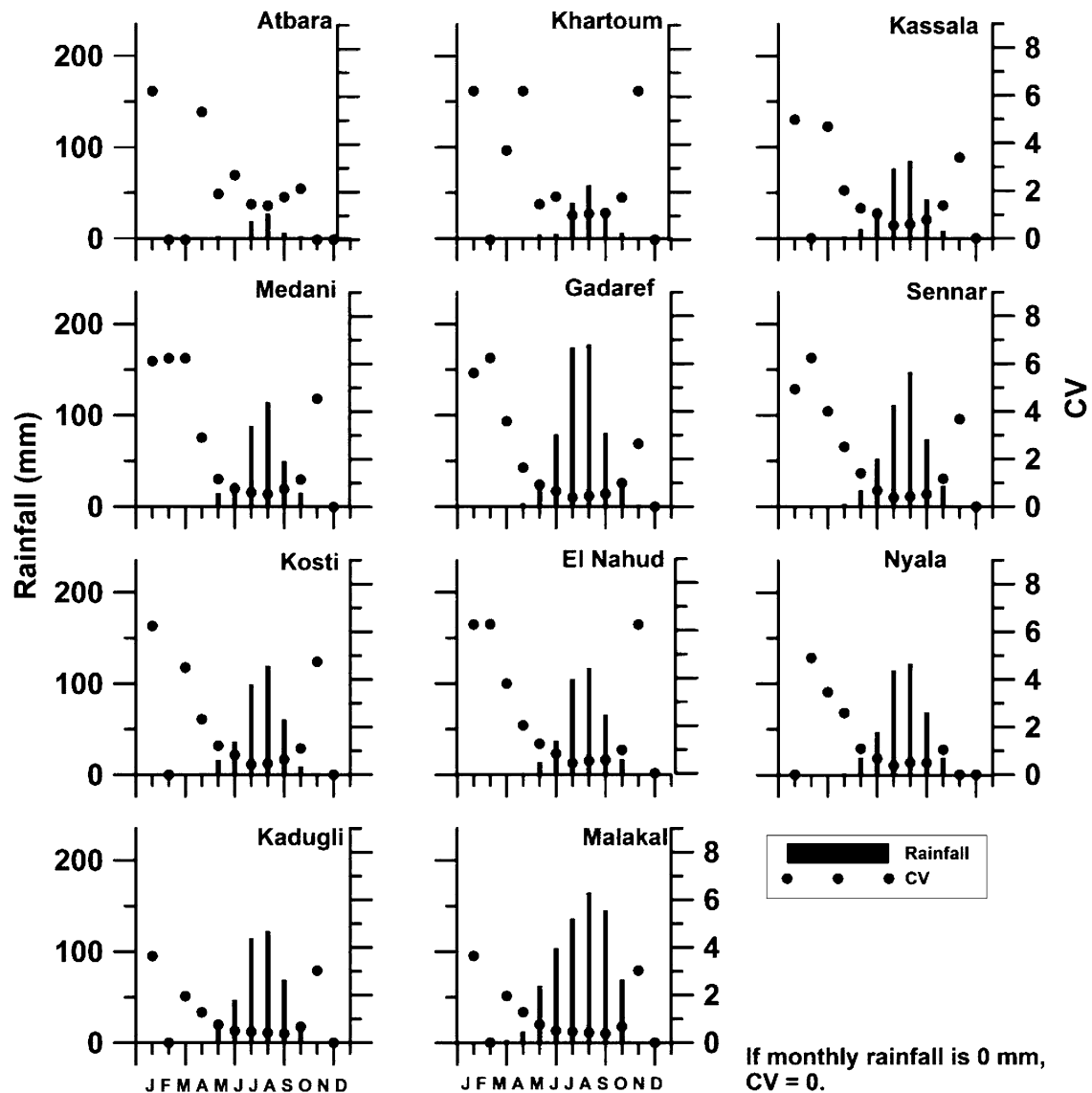


**Fig. 3** Histograms showing mean monthly rainfall and its coefficient of variation (CV)

16°N), and coastal region (Red Sea coast). Latitudes 9°–10° and 16°–17° approximately match annual rainfall isohyets of 600–800 and 200 mm, respectively. Latitude 9°–10° is the southern limit of the semiarid region, and latitude 16°–17° is the southern limit of the arid region.

We divided the study area into four zones on the basis of annual rainfall and cross-correlations among the rainfall time series of stations in each zone (Tables 2 and 3): Zone I

(annual rainfall less than 200 mm), Zone II (200–400 mm), Zone III (400–600 mm), and Zone IV (more than 600 mm). Table 3 presents the cross-correlations of rainfall time series between stations in each of these zones that exceeded 0.69. Our zoning scheme can be regarded as a subdivision of the desert, semi-desert, and savanna zones of Osman and Shamseldin (2002). Elagib (2010) assigned Kosti and Gadaref stations to the arid and semiarid zones, respectively. In the

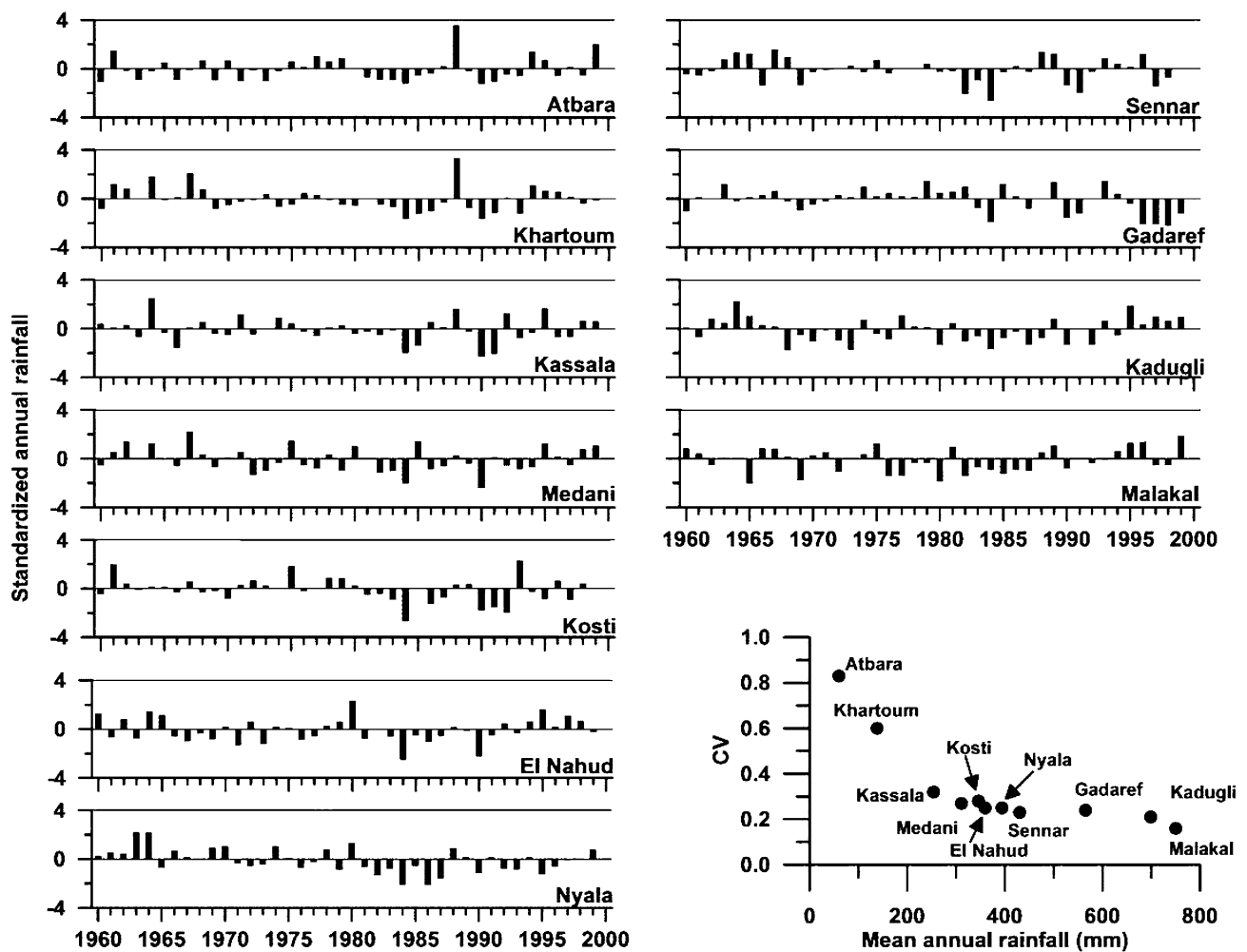


Fig. 4 Standardized annual rainfall for the 11 stations. The graph at the lower right plots mean annual rainfall against its coefficient of variation (CV) for 1960–1999

Table 2 Classification of mean annual rainfall of 11 rainfall stations

Zone	Zone I		Zone II			Zone III			Zone IV		
Station	Atbara	Khartoum	Kassala	Medani	Kosti	El Nahud	Nyala	Sennar	Gadaref	Kadugli	Malakal
Mean annual rainfall (mm)	59.8	138.1	253.9	311.1	346.0	359.6	394.2	430.5	565.5	699.0	750.4
Rainfall range (mm)	0–200		200–400			400–600			More than 600–		
CV	0.83	0.60	0.32	0.27	0.24	0.23	0.28	0.25	0.25	0.21	0.16

present study, Kosti and Gadaref are in Zone II and Zone III, respectively.

Zonal rainfall (Fig. 5) was obtained by averaging the rainfall of stations in that zone. All four zones had wet conditions in the early 1960s. In most of the 1980s, all zones had dry conditions, especially in 1984, while in 1988, extremely wet conditions occurred in Zone I (Bärring and Hulme 1991; Elagib and Elhag 2011).

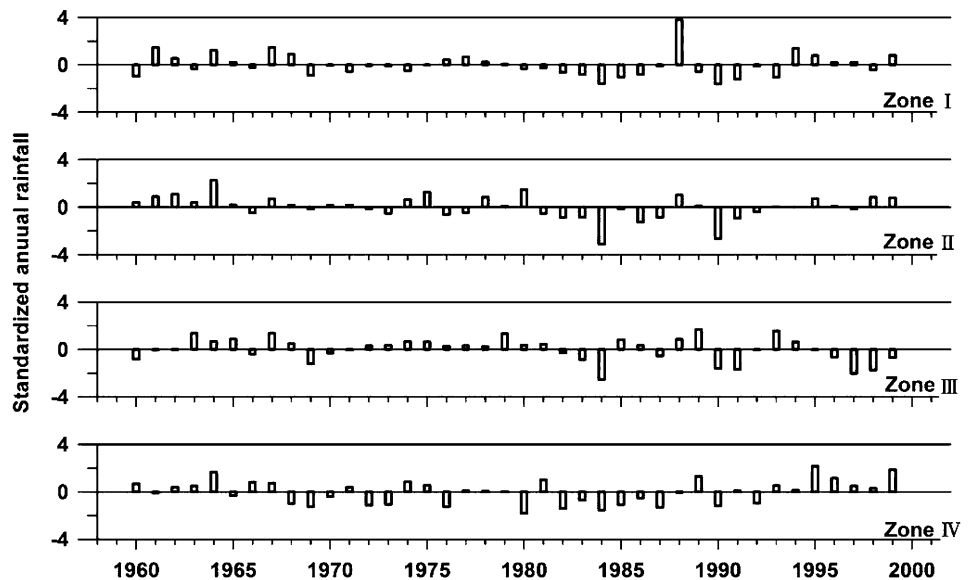
### Teleconnection with SST

#### Correlation between summer rainfall and the global SST field

Monthly rainfall in July and August (the peak of the rainy season) is shown in Fig. 3. We calculated cross-correlations

**Table 3** Cross-correlations of rainfall time series at gauging stations in four zones

Zone I					Atbara
Khartoum					0.691
Zone II		Kassala	Medani	Kosti	El Nahud
Medani	0.739	–	–	–	–
Kosti	0.719	0.775	–	–	–
El Nahud	0.755	0.777	0.764	–	–
Nyala	0.759	0.739	0.756	0.760	–
Zone III					Gadaref
Sennar					0.836
Zone IV					Kadugli
Malakal					0.735

**Fig. 5** Standardized annual rainfall of the four zones in the central Nile Basin

of the interannual time series of average combined July–August rainfall with the two-month average SST around the world ocean during various two-month periods with different time lags relative to July–August. For example, an average June–July value of SST was compared with average central Nile Basin rainfall in July and August, with a lag of 1 month.

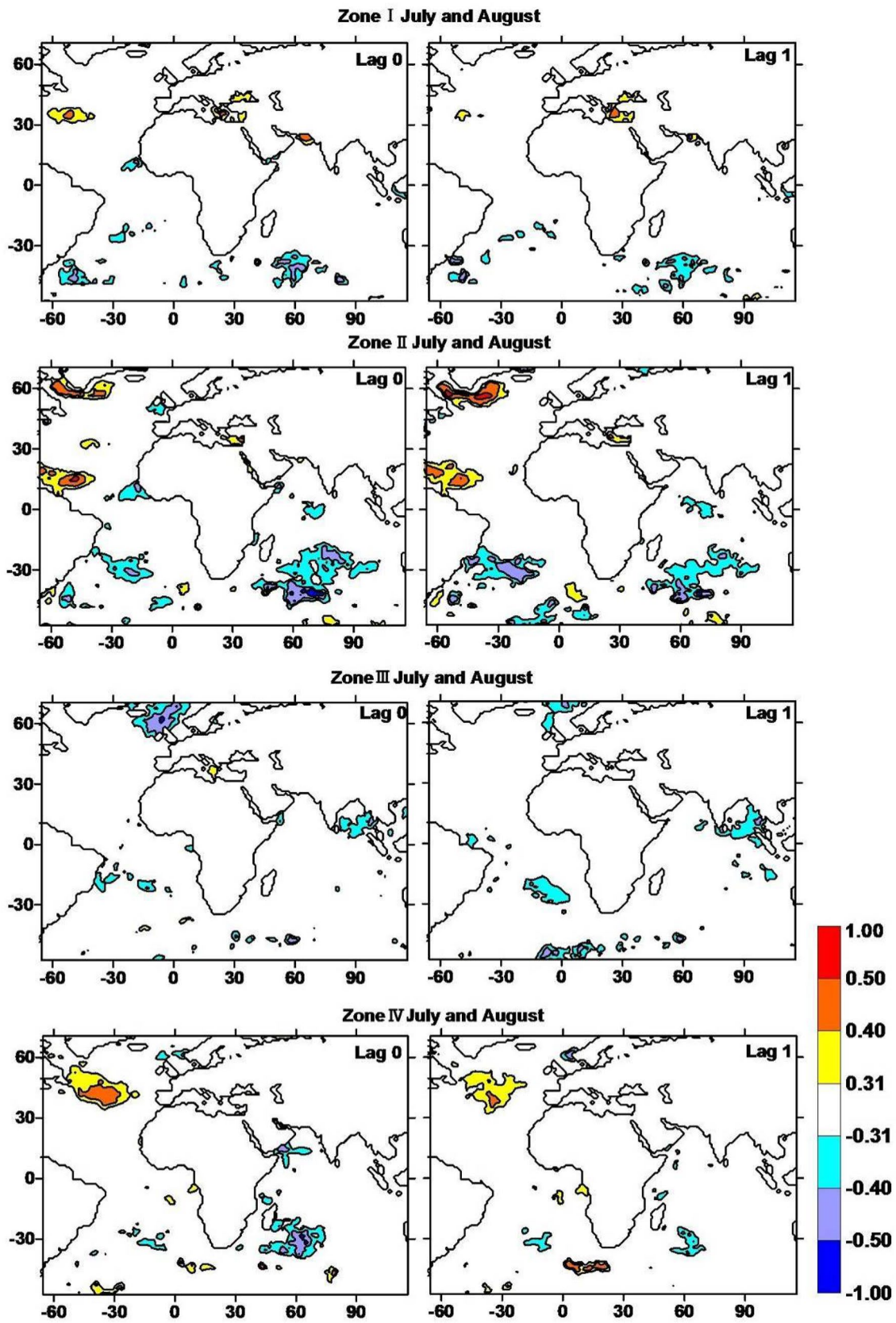
#### Cross-correlation for short lags (0 and 1 month)

Cross-correlations of summer rainfall in our four zones with SST in the Atlantic Ocean and Indian Ocean are shown in Fig. 6 for lag times of 0 month (left) and 1 month (right). Correlation values of 0.31, 0.40, and 0.50 correspond to significance levels of 0.05, 0.01, and 0.001, respectively.

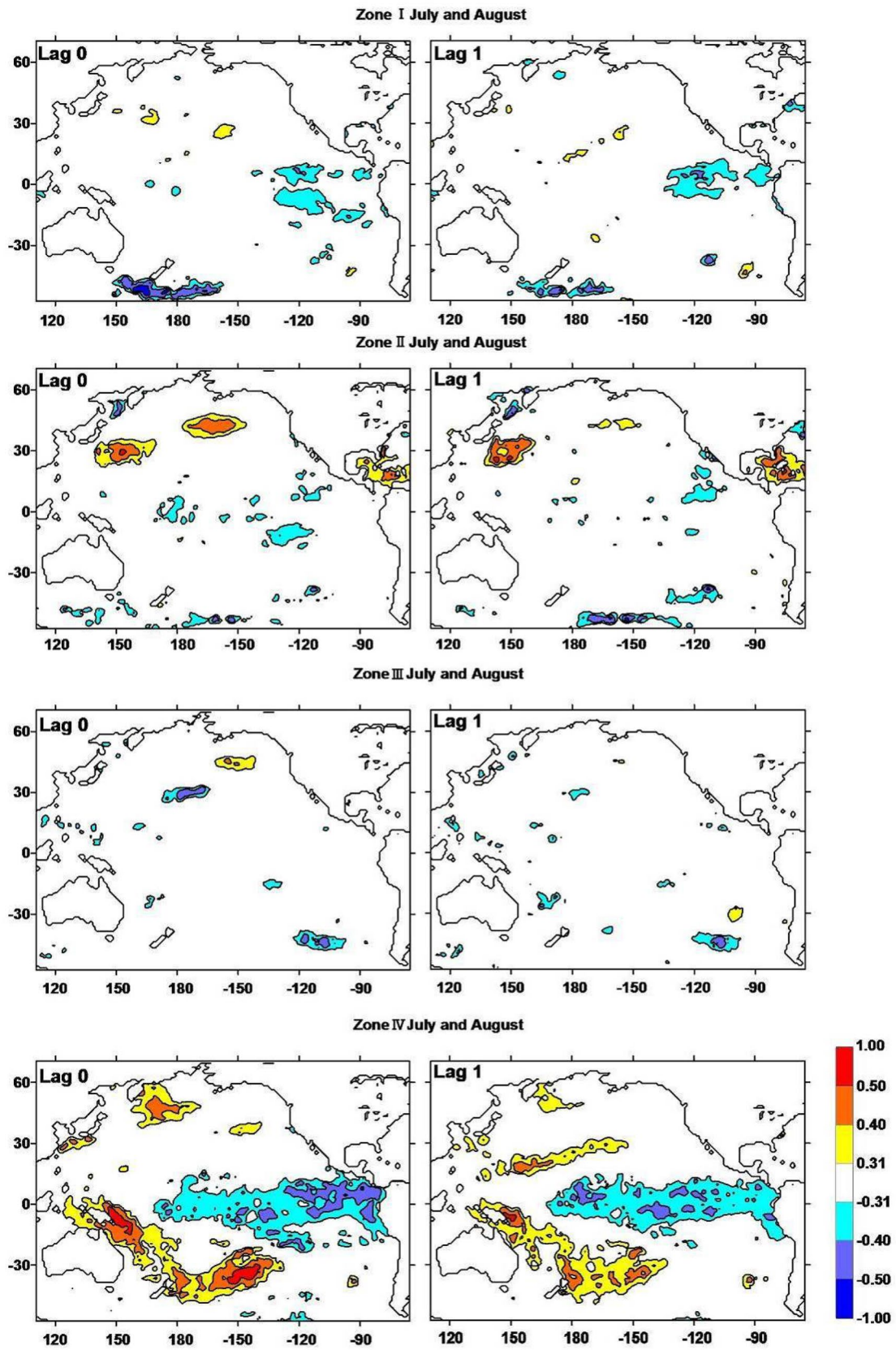
Significant positive cross-correlations with Zone I summer rainfall were found east of Newfoundland and in the eastern Mediterranean Sea, and negative ones were found south-east of Madagascar and east of Uruguay. Significant positive cross-correlations with Zone II summer rainfall were found south of Greenland, northeast of South America, and in the eastern Mediterranean Sea, and the negative ones were found east of Brazil, east of Uruguay, and in a broad area southeast of Madagascar. Zone III summer rainfall had negative correlations with SST around the Faeroe Islands, east of St. Helena, and in the Bay of Bengal. Zone IV summer rainfall had positive correlations with SST east of Newfoundland and southeast of Madagascar.

Figure 7 shows cross-correlations of summer rainfall in our four zones with SST in the Pacific Ocean for lag times





**Fig. 6** Map showing cross-correlations of central Nile Basin summer rainfall with SST in the Atlantic and Indian Ocean with a lag time of 0 or 1 month



**Fig. 7** Map showing cross-correlations of central Nile Basin summer rainfall with SST in the Pacific Ocean with a lag time of 0 or 1 month

of 0 month (left) and 1 month (right). Summer rainfall in Zone I had significant negative correlations with SST in the eastern equatorial Pacific Ocean and south of New Zealand. Zone II summer rainfall had significant positive and negative correlations with SST southeast and northeast of Japan, respectively. Zone III summer rainfall had significant positive and negative correlations west of South Africa and in the central Midway Islands, respectively. Zone IV summer rainfall had significant cross-correlations with SST over broad areas: negative ones in the central and eastern equatorial Pacific Ocean and positive ones from the north of Australia to east of New Zealand.

The SST changes over the eastern equatorial Pacific Ocean are well known as El Niño (higher temperature) and La Niña (lower temperature) events. The summer rainfall of Zone I (north) and IV (south) had negative correlations with SST in this region. It appears that La

Niña events are associated with higher rainfall in Zones I and IV.

### Cross-correlations at longer lags (3–6 months)

Possible teleconnections between rainfall and SST at longer lag times are most interesting from the standpoint of predicting. If a teleconnection can be established for some months, predictions of summer rainfall during that month could be possible. Cross-correlations of summer rain in the central Nile Basin with SST in the Atlantic and Indian Oceans are shown in Fig. 8 for lag times of 3 through 6 months. Correlations with Pacific Ocean SST are not significant, except that Zone IV has positive correlations with SST in Micronesia.

Zone I has significant positive correlations at 3- and 4-month lags with areas south of the Azores Islands and negative ones with the area south of Madagascar (Fig. 8).

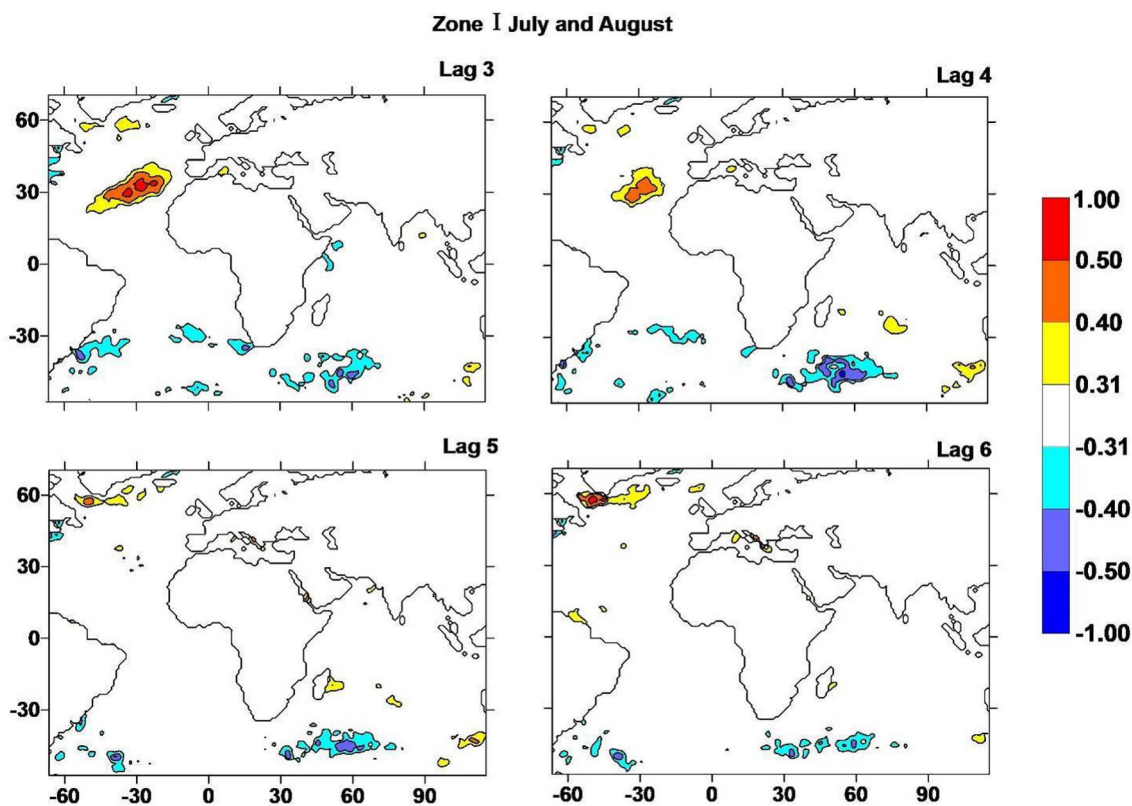


**Fig. 8** Cross-correlations of central Nile Basin summer rainfall in Zone I with SST in the Atlantic and Indian Ocean with a lag time of 3–6 months



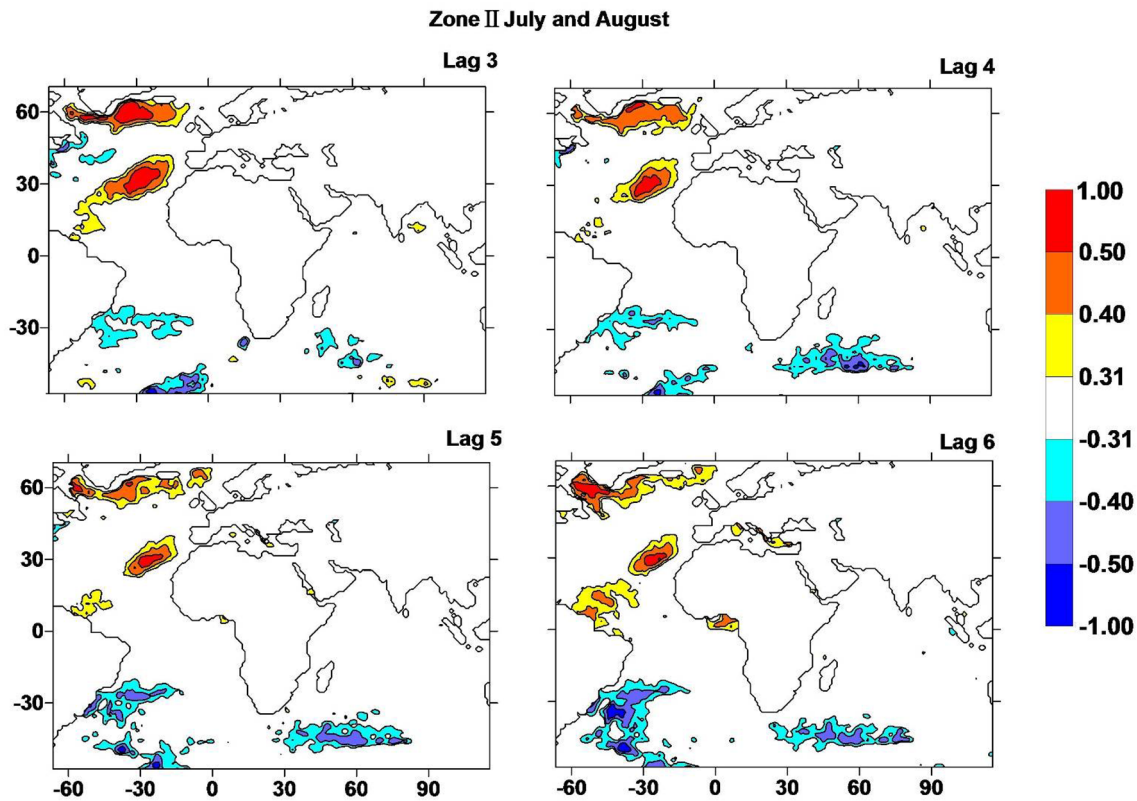


**Fig. 9** Cross-correlations of central Nile Basin summer rainfall in Zone II with SST over the Atlantic and Indian Ocean with a lag time of 3–6 months

Negative correlations are also found west and southwest of South Africa and south of Madagascar at other lag times.

Zone II has significant positive correlations at 3- and 4-month lags south of the Azores and east of Newfoundland (Fig. 9). It has significant negative correlations east of Brazil and south of Madagascar.

Unlike Zones I and II, Zone III does not have positive correlations with SST. Instead, it has significant negative correlations with SST of various regions in the Indian Ocean (Fig. 10). Zone IV has significant positive correlations with SST southwest of South Africa and Angola and significant negative correlations with SST in the southwestern Indian Ocean at 3–5-month lag (Fig. 11).

We extracted a set of ‘common SST regions’ that have significant correlations with summer rainfall in the central Nile Basin at a 2- or 3-month lag (Fig. 12). For Zone I at a

3- or 4-month lag, they are south of the Azores Islands (AZ), west of South Africa (AS), southwest of the South African coast (SASW), and south of Madagascar (MS). For Zone II at a 4–6-month lag, they are south of the Azores (AZ), east of Newfoundland (AN), east of Brazil (BE), and south of Madagascar (MS). For Zone III at a 3–6-month lag, it is the western Indian Ocean (INW). For Zone IV at a 3–5-month lag, they are southwest of South Africa (ASW) and Angola (ANG) and two regions (north and south) in the southwestern Indian Ocean (ISWN, ISWS).

### Cross-correlation of SST differences with rainfall

In addition to the correlations between summer rainfall time series of the four zones SST in parts of the Atlantic and Indian Oceans, in three cases we derived correlations

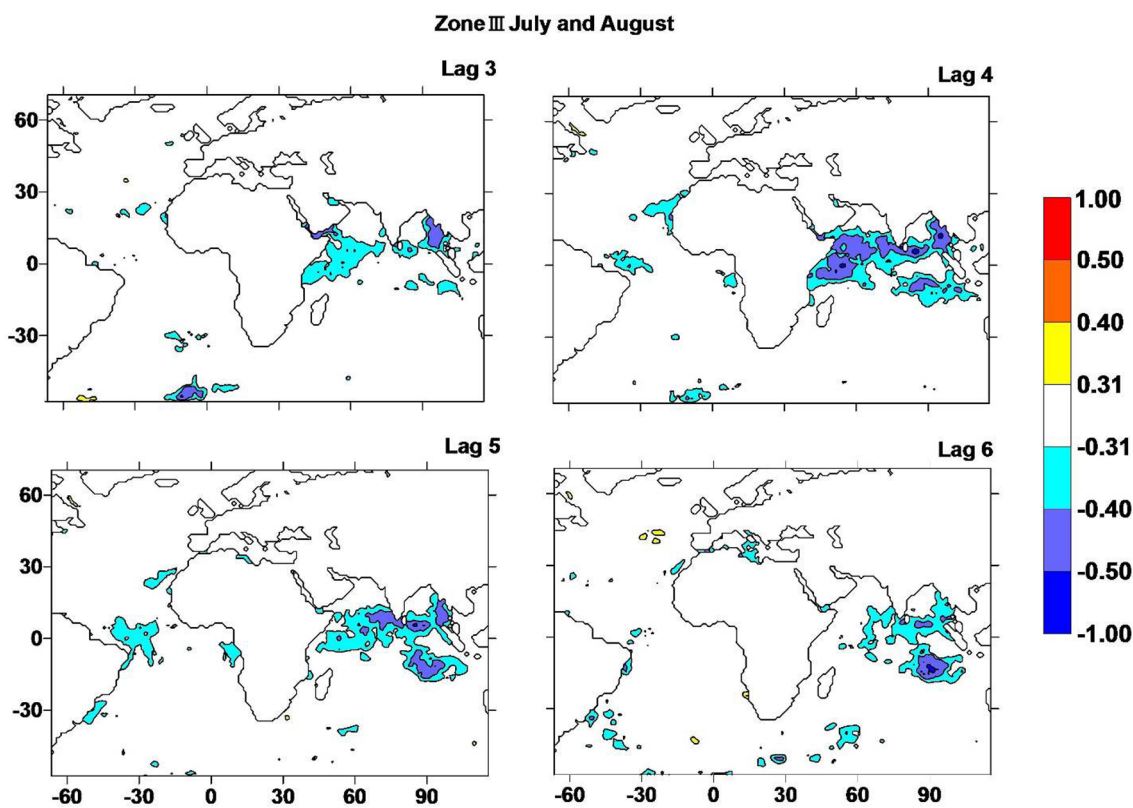


**Fig. 10** Cross-correlations of central Nile Basin summer rainfall in Zone III with SST over the Atlantic and Indian Ocean with a lag time of 3–6 months

between rainfall and the difference in SST between common SST regions (Fig. 12) that had opposite senses of correlation, positive and negative (Table 4).

Zone I had correlations of 0.492 and  $-0.368$  with SST in regions AZ and MS, respectively, with lag times of 3 or 4 months (Table 4). The correlation of Zone I rainfall with the SST difference between these two regions (AZ—MS) was 0.627. The correlation with the SST difference was at least 10% stronger than the correlation with either SST record alone.

Zone II had correlations of 0.535 and  $-0.505$  with SST in regions AZ and BE, respectively, with lag times of 4–6 months (Fig. 13). The correlation with the SST difference, 0.687, was at least 15% stronger than the correlation with either SST record alone.

Zone IV had correlations of 0.553 and  $-0.402$  with SST in regions ASW and ISWN, respectively, with lag times of 3–5 months (Table 4). The correlation with the SST difference was 0.583, at least 5% stronger than the correlation with either SST record alone.

### Prediction of summer rainfall

The SST difference time series had especially strong correlations (Table 4), and the lag times involved suggest the possibility of predicting the summer rainfall in the central Nile Basin several months in advance. We tested this possibility using an ANN.

In our ANN, the historical record of SST differences was applied as the input layer and the central Nile Basin summer

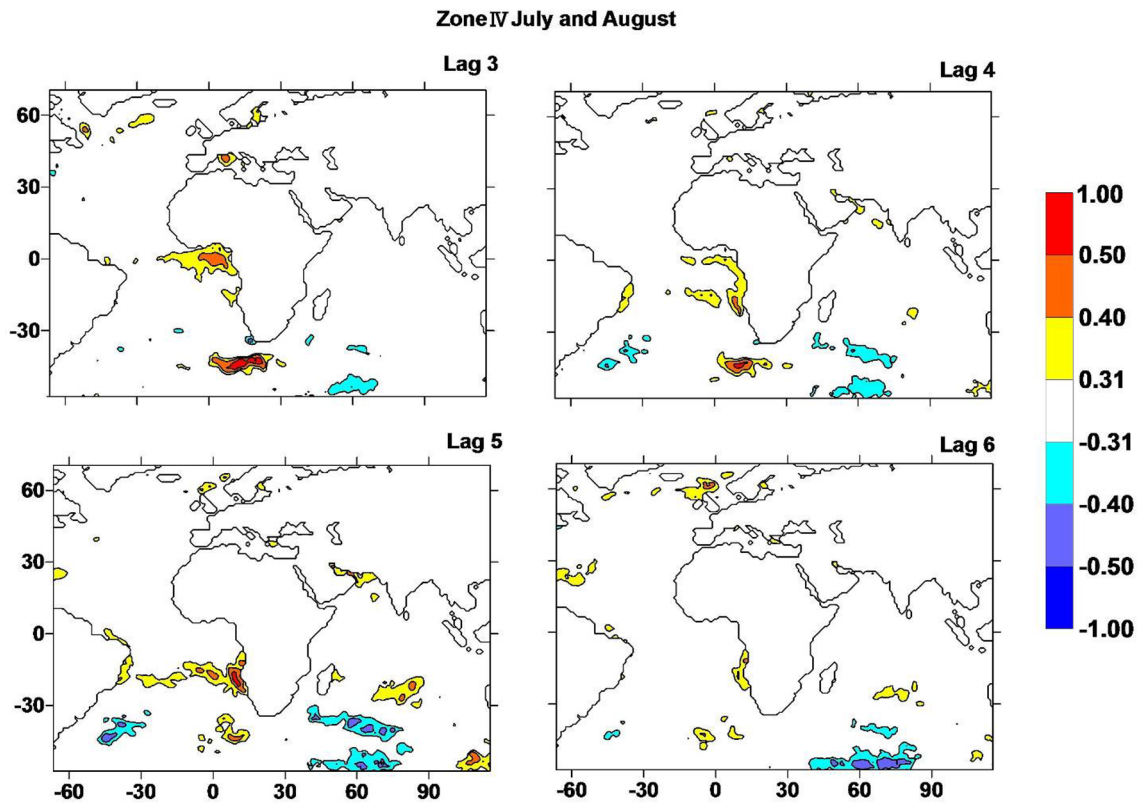


**Fig. 11** Cross-correlations of central Nile Basin summer rainfall in Zone IV with SST over the Atlantic and Indian Ocean with a lag time of 3–6 months

rainfall was the output layer. To match observed rainfall with the predicted rainfall from the output layer, a back-propagation algorithm was applied to optimize the weight functions (Yasuda et al., 2009). Out of 40 years (1960–1999) of available data on rainfall and SST, data from the first 28 years (1960–1979) were used for calibration and the data from the second 12 years were used for validation (e.g., Singh and Borah, 2013). On the calculation process of the ANN, interannual time series of the SST difference for 4–5 years were applied to the input layer and interannual time series of the summer rainfall for 1–2 years was fitted to the output layer. For the calibration process (first 20 years), the weights among the layers were optimized by the back-propagation and the optimized weights were applied to the validation process to fit the predicted summer rainfall to observed ones.

The observed and predicted summer rainfall for Zones I, II, and IV, presented in Fig. 14, had a correlation coefficient greater than 0.70.

## Conclusion

Eleven rainfall stations in the central Nile Basin in Sudan, extending from the northern arid area to the southern wet area, were classified into four zones on the basis of mean annual rainfall and cross-correlations among the stations within each zone. At all of the stations, dry and rainy seasons are very distinct, as indicated clearly by the PCI and SI indices, with the rainy season being limited to July and August. Cross-correlations of summer rainfall in these four zones with the global



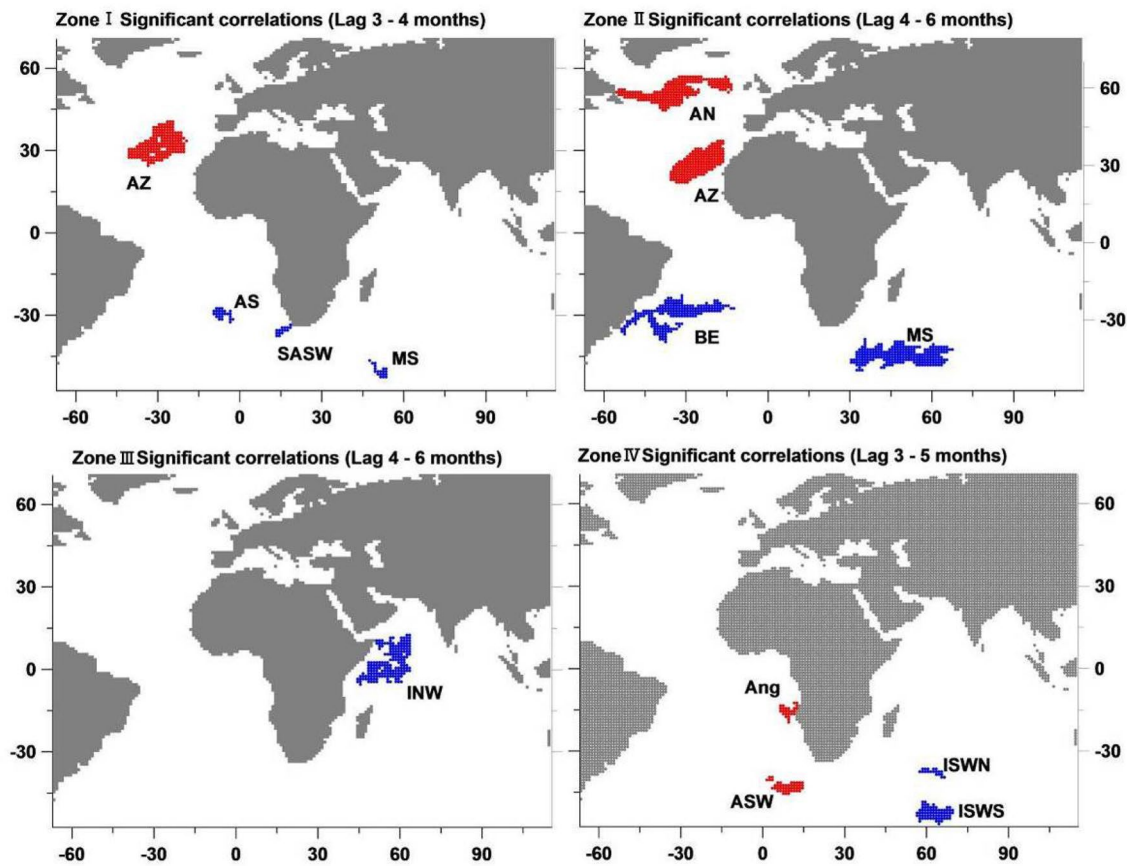


**Fig. 12** Extraction of SST zones having significant correlation ( $|r| > 0.31$ ; red is positive and blue is negative) with central Nile Basin summer rainfall at the specified lag time. (Color figure online)

**Table 4** Correlations of SST and SST difference zones

Zone I	AZ	MS	SASW	AS	Difference (AZ-MS)
Lag 3–4 months	0.492	−0.368	−0.397	−0.368	0.627
Zone II	AZ	AN	BE	MS	Difference (AZ-BE)
Lag 4–6 months	0.535	0.502	−0.505	−0.480	0.687
Zone III	INW				–
Lag 4–6 months	−0.371				
Zone IV	ASW	Ang	ISWN	ISWS	Difference (ASW-ISWN)
Lag 3–5 months	0.553	0.406	−0.402	−0.426	0.583

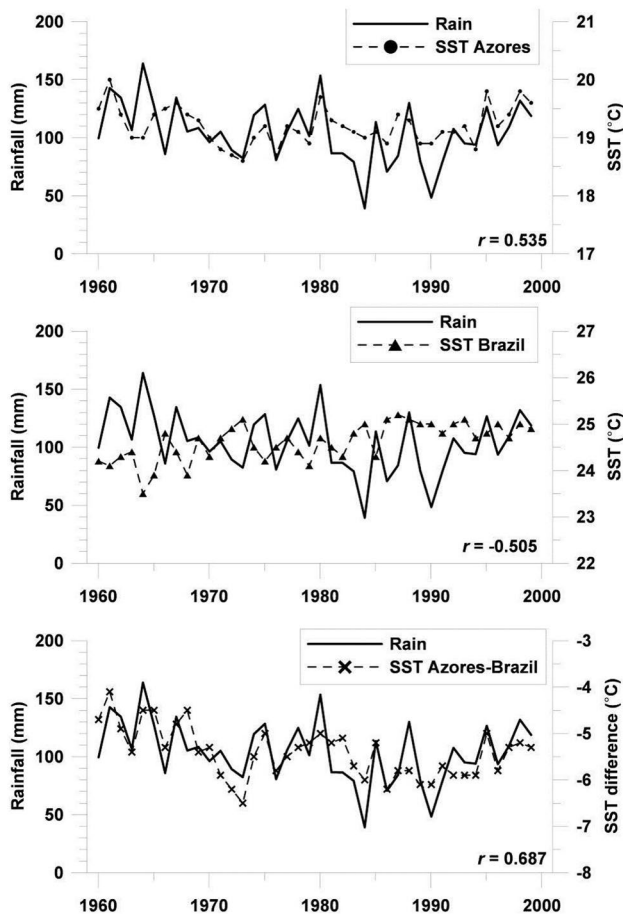


**Fig. 13** Time series of SST in the Azores and Brazil common SST regions (top and middle) and the SST difference between them (bottom), plotted with summer rainfall in Zone II

SST field were calculated. Correlations were significant with SST in the Pacific Ocean at short lag times (0 and 1 month), but not at longer lag times (3–6 months); instead, correlations were significant with SST in parts of the Atlantic and Indian Oceans. For three pairs of these SST regions with positive and negative correlations, the difference in SST within the pair was more strongly correlated with the Nile Basin rainfall than either region alone. In a test of an ANN to predict summer rainfall from these SST differences several months in advance, the SST differences were applied at the input layer and the summer rainfall was predicted at the output layer. The observed and predicted summer rainfall values from the ANN model had correlation coefficients greater than 0.70.

**Acknowledgements** The authors gratefully acknowledge financial support by the Science Research project of the Japan Society for the Promotion of Science (No. 23404014) and the Joint Research Program of the Arid Land Research Center, Tottori University.

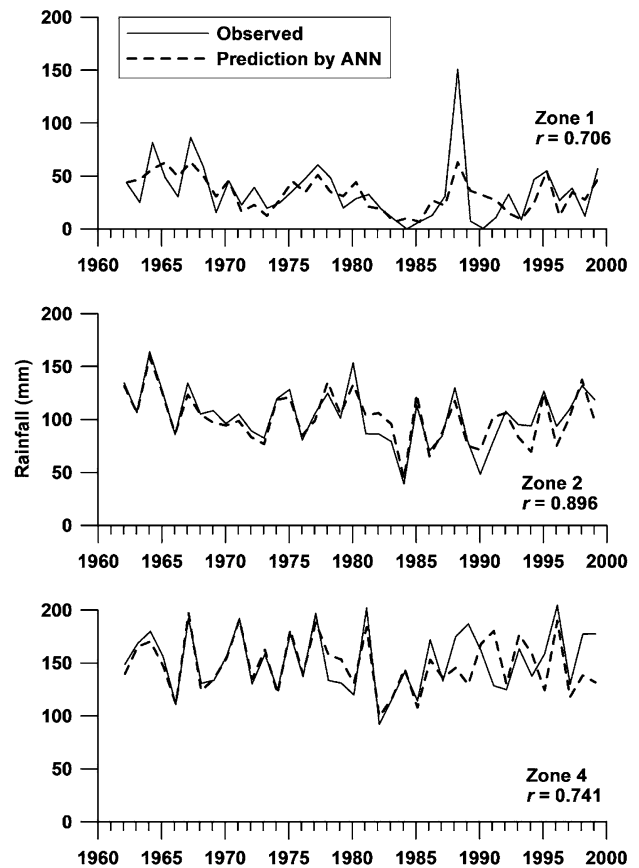


**Fig. 14** Time series of observed and predicted summer rainfall in Zones I, II, and IV

## References

- Apaydin H, Erpul G, Bayramin I, Gabriels D (2006) Evaluation of indices for characterizing the distribution and concentration of precipitation: a case for the region of South-eastern Anatolia Project, Turkey. *J Hydrol* 328:726–732
- Ayoade JO (1970) The seasonal incidence of rainfall. *Weather* 25:414–418
- Bärring L, Hulme M (1991) Filters and approximate confidence-interval for interpreting rainfall anomaly indexes. *J Clim* 4:837–847
- Behera S, Yamagata T (2001) Subtropical SST dipole events in the southern Indian ocean. *Geophys Res Lett* 28:327–330
- Bello NJ (1998) Evidence of climate change based on rainfall records in Nigeria. *Weather* 53:412–418
- Camberlin P (1997) Rainfall anomalies in the source region of the Nile and their connection with the Indian summer monsoon. *J Clim* 10:1380–1392
- Chen CJ, Georgakakos AP (2015) Seasonal prediction of East African rainfall. *Int J Climatol* 35:2698–2723. <https://doi.org/10.1002/joc.4165>

- Dash NB, Panda SN, Remesan R, Sahoo N (2010) Hybrid neural modeling for groundwater level prediction. *Nat Hazards Earth Syst Sci* 19:1251–1263
- de Luis M, Gonzalez-Hidalgo JC, Longares LA (2010) Is rainfall erosivity increasing in the Mediterranean Iberian Peninsula? *Land Degrad Dev* 21:139–144
- de Luis M, Gonzalez-Hidalgo JC, Brunetti M, Longares LA (2011) Precipitation concentration changes in Spain 1946–2005. *Nat Hazards Earth Syst Sci* 11:1259–1265
- Diro GT, Grimes DIF, Black E (2011) Teleconnections between Ethiopian summer rainfall and sea surface temperature: part I—observation and modelling. *Clim Dyn* 37:103–119
- Elagib NA (2010) Exploratory analysis of rain days in central Sudan. *Meteorol Atmos Phys* 109:47–59
- Elagib NA (2011) Changing rainfall, seasonality and erosivity in the hyper-arid zone of Sudan. *Land Degrad Dev* 22:505–512
- Elagib NA, Elhag MM (2011) Major climate indicators of ongoing drought in Sudan. *J Hydrol* 409:612–625
- Elagib NA, Mansell MG (2000) Climate impacts of environmental degradation in Sudan. *Geojournal* 50:311–327
- Fontaine B, Gaetani M, Ullmann A, Roucou P (2011) Time evolution of observed July–September sea surface temperature–Sahel climate teleconnection with removed quasi-global effect (1900–2008). *J Geophys Res.* <https://doi.org/10.1029/2010JD014843>
- Goyal MK, Ojha CSP (2012) Downscaling of surface temperature for lake catchment in an arid region in India using linear multiple regression and neural networks. *Int J Climatol* 32:552–566
- Hameed S, Riemer N (2012) Relationship of Sahel precipitation and atmospheric centers of action. *Adv Meteorol.* <https://doi.org/10.1155/2012/953853>
- Kumbuyo C, Yasuda H, Kitamura Y, Shimizu K (2014) Fluctuation of rainfall time series in Malawi. An analysis of selected areas. *Geofizika* 31:13–34. <https://doi.org/10.15233/gfz.2014.31.1>
- Larsson H (1996) Relationships between rainfall and sorghum, millet and sesame in the Kassala province, eastern Sudan. *J Arid Environ* 32:211–223
- Livada I, Asimakopoulos DN (2005) Individual seasonality index of rainfall regimes in Greece. *Clim Res* 28:155–161
- Michiels P, Gabries D, Hartmann R (1992) Using the seasonal and temporal precipitation concentration index for characterizing the monthly rainfall distribution in Spain. *CATENA* 19:43–58
- Middleton N, Thomas D (1997) *World atlas of desertification*. Wiley, New York
- Nicholson SE (2011) *Dryland climatology*. Cambridge University Press, Cambridge, pp 196–200
- Nilsson P, Cintia BU, Berndtsson R (2006) Monthly runoff simulation: comparing and combining conceptual and neural network models. *J Hydrol* 321:344–363
- Oliver JE (1980) Monthly precipitation distribution: a comparative index. *Prof Geogr* 32:300–309
- Olsson J, Uvo CB, Jinno K (2001) Statistical atmospheric downscaling of short-term extreme rainfall by neural networks. *Phys Chem Earth Part B Hydrol Oceans* 26:695–700
- Osman YZ, Shamseldin AY (2002) Qualitative rainfall prediction models for central and southern Sudan using El Niño—Southern Oscillation and Indian Ocean sea surface temperature indices. *Int J Climatol* 22:1861–1878
- Pryor SC, Schoof JT (2008) Changes in precipitation seasonality over the contiguous USA. *J Geophys Res Atmos.* <https://doi.org/10.1029/2008JD010251>
- Rayner NA, Parker DE, Horton EB, Folland CK, Alexander LV, Rowell DP, Kent EC, Kaplan A (2003) Global analyses of sea surface temperature, sea ice, and night marine air temperature since the late nineteenth century. *J Geophys Res.* <https://doi.org/10.1029/2002JD002670>
- Rayner NA, Brohan P, Parker DE, Folland CK, Kennedy JJ, Vanicek M, Ansell T, Tett SFB (2006) Improved analyses of changes and uncertainties in sea surface temperature measured in situ since the mid-nineteenth century: the HadSST2 data set. *J Clim* 19:446–469
- Rishmawi K, Prince SD, Xue YK (2016) Vegetation responses to climate variability in the northern arid to sub-humid zones of Sub-Saharan Africa. *Remote Sens* 8:910. <https://doi.org/10.3390/rs8110910>
- Rodríguez-Fonseca B, Polo I, Serrano E, Castro M (2006) Evaluation of the north Atlantic SST forcing on the European and Northern African winter climate. *Int J Climatol* 26:179–191
- Saji NH, Yamagata T (2003) Possible impacts of Indian Ocean dipole mode events on global climate. *Clim Res* 25:151–169
- Shankar D, Shetye SR, Joseph PV (2007) Link between convection and meridional gradient of sea surface temperature in the Bay of Bengal. *J Earth Syst Sci* 116:385–406
- Singh P, Borah B (2013) Indian summer monsoon rainfall prediction using artificial neural network. *Stoch Env Res Risk A* 27:1585–1599
- Smith IN, McIntosh P, Ansell TJ, Reason CJC, McInnes K (2000) Southwest western Australian winter rainfall and its association with ocean climate variability. *Int J Climatol* 20:1913–1930
- Srivastava P, McNair JN, Johnson TE (2006) Comparison of process-based and artificial neural network approaches for stream flow modeling in an agricultural watershed. *J Am Water Resour Assoc* 42:545–563
- Sumner G, Homar V, Ramis C (2001) Precipitation seasonality in eastern and southern coastal Spain. *Int J Climatol* 21:219–247
- Traore S, Zerbo L, Schmidt M, Thiombiano L (2012) Acacia communities and species responses to soil and climate gradients in the Sudano-Sahelian zone of West Africa. *J Arid Environ* 87:144–152
- Uvo CB, Repelli CA, Zebiak SE, Kushnir Y (1998) The relationships between tropical Pacific and Atlantic SST and northeast Brazil monthly precipitation. *J Clim* 11:551–562
- Uvo CB, Tolle U, Berndtsson R (2000) Forecasting discharge in Amazonia using artificial neural networks. *Int J Climatol* 20:1495–1507
- Willcocks TJ, Twomlow SJ (1992) An evaluation of sustainable cultural practices for rainfed sorghum production on Vertisols in east Sudan. *Soil Till Res* 24:183–198
- World Meteorological Organization (2004) *Forecasting El Niño: science's gift to the twenty-first century*. World Climate Programme, Africa. Flip Side of Science, 39p
- Yasuda H, Berndtsson R, Saito T, Anyoji H, Zhang X (2009) Prediction of Chinese Loess plateau summer rainfall using Pacific Ocean spring sea surface temperature. *Hydrol Process* 23:719–729
- Yuan F, Yasuda H, Berndtsson R, Uvo CB, Zhang L, Hao Z, Wang X (2015) Regional sea surface temperatures explain spatial and temporal variation of summer precipitation in the source region of the Yellow River. *Sci J, Hydrol.* <https://doi.org/10.1080/02626667.2015.1035658>
- Zheng J, Li J, Feng J (2014) A dipole pattern in the Indian and Pacific oceans and its relationship with the East Asian summer monsoon. *Res Lett, Env.* <https://doi.org/10.1088/1748-9326/9/7/074006>